Sustained oscillations accompanying polarization switching in laser dynamics

Chi-Hak Uy, Lionel Weicker, Damien Rontani, Marc Sciamanna

Sustained oscillations accompanying polarization switching in laser dynamics

CHI-HAK UY,[1,2,*] LIONEL WEICKER,[1,2] DAMIEN RONTANI,[1,2] AND MARC SCIAMANNA[1,2]

[1]*Chaire Photonique, CentraleSupélec, F-57070 Metz, France*
[2]*LMOPS EA 4423 Laboratory, CentraleSupélec and Université de Lorraine, F-57070 Metz, France*
*chi-hak.uy@centralesupelec.fr

Abstract: We report experimentally and theoretically the emergence of sustained oscillations over a slow and periodic polarization switching in a laser subjected to polarization rotated optical feedback. This phenomenon originates from a clear bifurcation point that marks the transition between sustained and damped oscillations on the plateaus. Analytical study reveals also that the frequency of this new oscillatory dynamics is independent of the time delay.

OCIS codes: (250.5960) Semiconductor lasers; (140.1540) Chaos.

References and links

1. K. Panajotov, B. Ryvkin, J. Danckaert, M. Peeters, H. Thienpont, and I. Veretennicoff, "Polarization switching in VCSEL's due to thermal lensing," IEEE Photonic. Tech. Lett. **10**(1), 6–8 (1998).
2. M. Virte, K. Panajotov, H. Thienpont, and M. Sciamanna, "Deterministic polarization chaos from a laser diode," Nat. Photonics **7**(1), 60 (2013).
3. I. Gatare, M. Sciamanna, J. Buesa, H. Thienpont, and K. Panajotov, "Nonlinear dynamics accompanying polarization switching in vertical-cavity surface-emitting lasers with orthogonal optical injection," Appl. Phys. Lett. **88**(10), 101–106 (2006).
4. Y. Hong, KA. Shore, A. Larsson, M. Ghisoni, and J. Halonen, "Polarisation switching in a vertical cavity surface emitting semiconductor laser by frequency detuning," IEEE Proc. Optoelectron. **148**(1), 31–34 (2001).
5. K. Panajotov, F. Berghmans, M. Peeters, G. Verschaffelt, J. Danckaert, I. Veretennicoff, and H. Thienpont, "Data transparent reconfigurable optical interconnections using polarization switching in VCSEL's induced by optical injection," IEEE Phot. Tech. Lett. **11**(8), 985–987 (1999).
6. H. Kawaguchi, T. Mori, Y. Sato, and Y. Yamayoshi, "Optical buffer memory using polarization-bistable vertical-cavity surface-emitting lasers," Jpn. J. Appl. Phys. **45**(9L), L894 (2006).
7. I. Gatare, M. Sciamanna, A. Locquet, and K. Panajotov, "Influence of polarization mode competition on the synchronization of two unidirectionally coupled vertical-cavity surface-emitting lasers," Opt. Lett. **32**(12),1629–1631 (2007).
8. M. Virte, E. Mercier, H. Thienpont, K. Panajotov, and M. Sciamanna, "Physical random bit generation from chaotic solitary laser diode," Opt. Express **22**(14), 17271–17280 (2014).
9. M. Sciamanna, K. Panajotov, H. Thienpont, I. Veretennicoff, P. Megret, and M. Blondel, "Optical feedback induces polarization mode hopping in vertical-cavity surface-emitting lasers," Opt. Lett. **28**(17), 1543–1545 (2003).
10. A. Karsaklian Dal Bosco, N. Sato, Y. Terashima, S. Ohara, A. Uchida, T. Harayama, and M. Inubushi, "Random number generation from intermittent optical chaos," IEEE J. Sel. Top. Quant. (2017).
11. A. Gahl, S. Balle and MS. Miguel, "Polarization dynamics of optically pumped VCSELs," IEEE J. Quantum Elect. **35**(3), 342–351 (1999).
12. H. Höpfner, M. Lindemann, N. Gerhardt, and M. Hofmann, "Controlled switching of ultrafast circular polarization oscillations in spin-polarized vertical-cavity surface-emitting lasers," Appl. Phys. Lett. **104**(2), 022409 (2014).
13. F. Denis-le Coarer, A. Quirce, A. Valle, L. Pesquera, L. Presquera, M. Sciamanna, H. Thienpont, and K. Panajotov, "Polarization dynamics induced by parallel optical injection in a single-mode VCSEL," Opt. Lett. **42**(11), 2130–2133 (2017).
14. S. Jiang, Z. Pan, M. Daganais, R. A. Morgan, and K. Kojima, "High-frequency polarization self-modulation in vertical-cavity surface-emitting lasers," Appl. Phys. Lett. **63**(26), 3545–3547 (1993).
15. M. Sciamanna, T. Erneux, F. Rogister, O. Deparis, P. Megret, and M. Blondel, "Bifurcation bridges between external-cavity modes lead to polarization self-modulation in vertical-cavity surface-emitting lasers," Phys. Rev. A **65**(4), 041801 (2002).
16. A. Gavrielides, T. Erneux, D. Sukow, G. Burner, T. McLachlan, J. Miller, and J. Amonette,"Square-wave self-modulation in diode lasers with polarization-rotated optical feedback," Opt. Lett. **31**(13), 2006–2008 (2006).

17. A. Gavrielides, D. Sukow, G. Burner, T. McLachlan, J. Miller, and J. Amonette, "Simple and complex square waves in an edge-emitting diode laser with polarization-rotated optical feedback," Phys. Rev. E **81**(5), 056209 (2010).
18. D. Sukow, T. Gilfillan, B. Pope, M. Torre, A. Gavrielides, and C. Masoller, "Square-wave switching in vertical-cavity surface-emitting lasers with polarization-rotated optical feedback: Experiments and simulations," Phys. Rev. A **86**(3), 033818 (2012).
19. M. Marconi, J. Javaloyes, S. Barland, M. Guidici, and S. Balle, "Robust square-wave polarization switching in vertical-cavity surface-emitting lasers," Phys. Rev. A **87**(1), 013827 (2013).
20. G. Friart, L. Weicker, J. Danckaert, and T. Erneux, "Relaxation and square-wave oscillations in a semiconductor laser with polarization rotated optical feedback," Opt. Express **22**(6), 6905–6918 (2014).
21. G. Friart, G. Verschaffelt, J. Danckaert, and T. Erneux, "All-optical controlled switching between time-periodic square waves in diode lasers with delayed feedback," Opt. Lett. **39**(21), 6098–6101 (2014).
22. R. Lang and K. Kobayashi, "External optical feedback effects on semiconductor injection laser properties," IEEE J. Quantum Elect. **16**(3), 347–355 (1980).
23. T. Heil, A. Uchida, P. Davis, and T. Aida, "TE-TM dynamics in a semiconductor laser subject to polarization-rotated optical feedback," Phys. Rev. A **68**(3), 033811 (2003).
24. M. Arteaga, H. Unold, J. Ostermann, R. Michalzik, and H. Thienpont, and K. Panajotov "Investigation of polarization properties of VCSELs subject to optical feedback from an extremely short external cavity-Part I: Theoretical analysis," IEEE J. Quantum Elect. **42**(2), 89–101 (2006).
25. D. Sukow, A. Gavrielides, T. Erneux, B. Mooeyhan, K. Lee, J. Mckay, and J. Davis, "Asymmetric square waves in mutually coupled semiconductor lasers with orthogonal optical injection," Phys. Rev. E **81**(2), 025206 (2010).
26. J. Javaloyes and S. Balle, "All-optical directional switching of bistable semiconductor ring lasers," IEEE J. Quantum Elect. **47**(8), 1078–1085 (2011).

1. Introduction

Semiconductor lasers usually emit linearly polarized light due to the symmetry of their gain medium and their inherent material anisotropy. However, modifying the semiconductor structure and operating parameters [1, 2] or applying an external perturbation [3, 4] may induce a switch towards an orthogonal polarization state. In addition, although being detrimental in e.g. optical communication, polarization switching found interest in optical routing [5], clock recovery [6], secure communication [7], and random number generation [8]. Randomly occurring switching can be triggered by noise [9] or inherent to a chaotic dynamic [10]. On the other hand, periodic switching can be achieved through optical pulse pumping [11, 12] and optical injection [13], and with polarization rotation of a feedback light [14–21]. In this last configuration two different setups have been considered: one where each of the orthogonal polarizations is reinjected in the laser after being turned by 90° and an other one where one polarization is filtered while the other one is turned by 90°. In the following, we focus on the setup with filtering of one polarization that has been called in [16] *Polarization rotated optical feedback* (PROF) and also referred as *cross-polarization reinjection* in [19]. Polarization switching in PROF arises from a Hopf bifurcation creating a square-wave modulation in long-cavity regime [17, 20]. Some studies have observed that the switchings are usually accompanied with highly damped oscillations at the internal relaxation oscillation frequency f_{RO} of the laser [16, 20].

In this study, we experimentally generate square-wave (SW) polarization switching with a PROF configuration and show for the first time not damped but sustained oscillation on the upper and lower level of the SWs. Although such oscillations have been found in numerical simulation of VCSEL with PROF, they were never observed experimentally. Furthermore, an in-depth bifurcation analysis shows that these oscillation are not sustained relaxation oscillation as implied in [18] but limit cycle dynamic at a frequency different from both f_{RO} and the external cavity frequency f_{EC} (the inverse of the round-trip time in the feedback arm).

2. Experimental results

The experimental setup, sketched in Fig. 1, comprises an edge-emitting laser (EEL) JDS SDL-5400 at 852 nm. We operate at 60 mA (four times the threshold current) and at 25^oC. The beam is collimated and sent into two arms with a 30/70 beam-splitter allowing for a maximum feedback
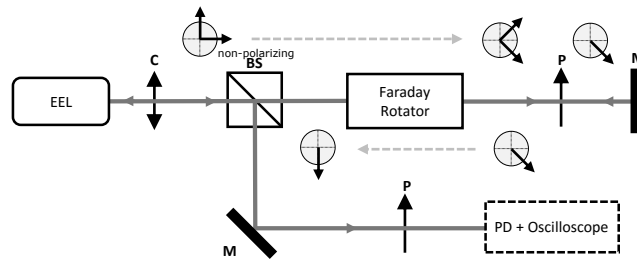
Fig. 1. Experimental setup. EEL : Edge-Emitting Laser, C : Collimator, BS : non-polarizing beamsplitter, P : polarizer, M : mirror, PD : photodiode. The polarization state of the laser signal is schematically represented on the light path.
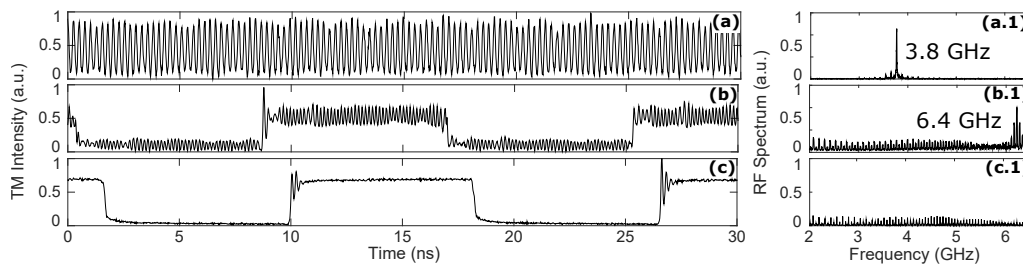

Fig. 2. Experimental time series of the TM modes for (a) 20%, (b) 29.8%, (c) 37% of feedback ratio. (a.1), (b.1) and (c.1) are the respective RF spectra. The delay is fixed at 8 ns.

ratio of 49%. The feedback ratio is deduced from the calibration of the attenuation wheel inserted just before the Faraday rotator and from the knowledge of the transmittance of the beam-splitter. A Faraday rotator is inserted in the external cavity and turns both TE and TM polarizations by 45°. The TM mode is then filtered with a polarizer while the mirror reflects the TE mode to the rotator, which turns again the polarization by 45°. As a result, the TE mode is injected in the laser with the same direction as the TM mode. Such a configuration also ensures the total suppression of multi-round-trip effect. In the detection arm, we measure the dynamics of the TM mode with a 12 GHz bandwidth Newfocus 1554-B photodiode and a 36 GHz bandwidth Lecroy oscilloscope. The delay is set to $\tau = 8$ ns.

In Fig. 2, we show experimental time series of the normally depressed TM mode and the corresponding RF spectra for different values of the feedback ratio. For low level of feedback, the laser emits a constant intensity in the TE mode. Increasing the feedback strength leads to undamped relaxation oscillations of the output power at a frequency of about 3.8 GHz [Fig. 2(a) and (a.1)]. For higher feedback, the system exhibits first chaos and then switches to SW solutions with 2τ-periodicity accompanied by sustained fast oscillations on the plateaus [Fig. 2(b)]. The corresponding RF spectrum, shown in panel (b.1), highlights a frequency comb with a spacing of $f_{EC}/2 = 62.5$ MHz, i.e. harmonics of the SW oscillation frequency, and a frequency peak at 6.4 GHz related to the frequency of oscillations on the plateaus. An intense peak at $f_{EC}/2 = 62.5$ MHz is also observed but not shown here (for clarity purpose). We note that the frequency on plateau is neither close to f_{RO} nor to f_{EC} or any of their harmonics. Finally, for high values of feedback, oscillations on the plateaus become damped leaving only a 2τ-periodic SW [Fig. 2(c)]. The corresponding RF spectrum [Fig. 2(c.1)] does not show any significant peak anymore but only the aforementioned frequency comb. This last case in Fig. 2(c) matches earlier observations where the polarization switchings are accompanied by damped oscillations at f_{RO} [16, 20].

Here, we are interested on the experimentally observed SW solutions with undamped oscillations
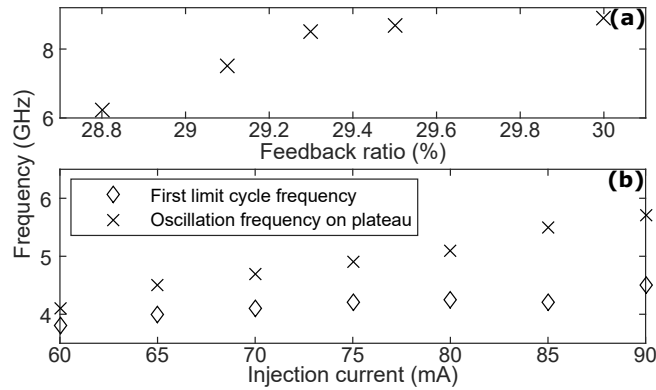
Fig. 3. Oscillation frequency on plateaus for (a) a current of 95 mA and increasing feedback ratio, (b) a feedback ratio of 28% and increasing current. In (b), comparison in shown with the frequency of the first limit-cycle dynamics for a feedback ratio of 20%.

on the plateaus and their frequencies and how they are influenced by tunable experimental parameters. In Fig. 3(a), we analyze first the effect of the feedback ratio. Compared to Fig. 2, we have increased the current to 95 mA so that the fast oscillations remain undamped in a larger span of feedback ratio. Although the uncertainty on the feedback ratio is fairly large (> 0.4%), we observe a clear increase of the fast oscillations frequency when increasing the feedback ratio. In Fig. 3(b), we then analyze the variations of the frequency on plateaus when varying the injection current. We compare it to the first observed limit-cycle frequency at low value of feedback ratio which we found in Fig. 2(a) as being close to the free-running f_{RO}. As we increase the current, the frequency of the first limit-cycle also increases similarly to the increase of f_{RO} with current. Besides, an increase of the oscillation frequency on plateaus is also observed when the current increases. This frequency remains always at a higher value than the first limit-cycle frequency and hence than f_{RO}. Finally, we have changed the delay from 8 ns to 12.9 ns but no significant change in the frequency of oscillation on plateaus has been observed, suggesting no dependence on f_{EC}.

3. Numerical results

We now focus on the transition between Fig. 2(c) and Fig. 2(b) where the high-frequency oscillations appear from the steady-state dynamic on the plateaus. The PROF setup can be modeled mathematically with a modified Lang-Kobayashi model [22, 23] that takes into account both the laser TE and TM modes. Although the importance of multiple round-trips has been highlighted in [24], our experimental configuration ensures that a single round-trip is experienced by the feedback beam. We therefore keep the model in its simplest form. As the TM mode is always filtered after the Faraday rotator and the delayed TE mode aligned with the original TM mode direction, the output TE field does not experience any feedback term. The model hence reads as follows

$$\dot{E}_1 = (1 + i\alpha)NE_1 + n_1, \tag{1}$$

$$\dot{E}_2 = (1 + i\alpha)k(N - \beta)E_2 + \eta\sqrt{k}E_1(s - \theta) + n_2, \tag{2}$$

$$T\dot{N} = P - N - (1 + 2N)[|E_1|^2 + |E_2|^2], \tag{3}$$

where $E_{1,2}$ are the TE and TM fields, respectively. s is the time normalized by the photon lifetime τ_p. N is the carrier density, $\theta = \tau/\tau_p$ the normalized delay, α the linewidth enhancement factor, η the feedback rate, T the ratio of carrier to cavity lifetime, k the gain coefficient ratio between

the TM and TE modes, $\beta = \frac{1}{2k}(1-k)$ the TM mode additional losses, and P the pump parameter above threshold. The terms $n_j = \sqrt{R}\xi_j$ ($j = 1, 2$) in Eq. 1 and Eq. 2 model two uncorrelated white Gaussian noises with variance R and zero mean.

For the sake of comparison with existing literature on PROF [16, 20, 21, 25], we considered very similar parameters : $P = 0.6$, $k = 0.96$, $\beta = 0.02$, $T = 250$, $\alpha = 2$ and $R = 10^{-12}$. We have fixed $\theta = 7000$, which matches the experimental delay value $\tau = 8$ ns when considering a realistic value for laser diodes $\tau_p = 1.14$ ps. For our parameters, the dimensionless free-running f_{RO} is given by $f_{RO} = 1/(2\pi) \times \sqrt{2P/T} = 0.011$ or 9.64 GHz for $\tau_p = 1.14$ ps. The need of comparison with previous bifurcation analyses gives here a different value of f_{RO} compared to the experiment. However, one can still adjust the parameters to obtain the experimental value of f_{RO} and the observed bifurcation scenario remains qualitatively very similar to the one reported here. In addition, although we have experimentally estimated the feedback ratio, the coupling efficiency of the feedback light into the laser cavity is unknown and therefore the feedback rate η remains a free bifurcation parameter.

Using these parameters, we show in Fig. 4(a) the bifurcation diagram with η as the bifurcation parameter. For low values of η, we observe a stable steady-state. Increasing η leads to a first bifurcation H_1 at $\eta = 0.013$ resulting in oscillatory dynamics at $f_{RO} = 0.011$ [see Fig. 4(b) and its zoom in panel (f)]. For $0.0336 < \eta < 0.0345$, the laser switches into quasi-periodicity and further into a narrow region of chaos. Increasing the value of η leads to 2θ-periodic SW with fast oscillations on both plateaus [see Fig. 4(c)]. The oscillations on the lower state completely disappear from $\eta > 0.05$ but the upper state oscillations still remain [see Fig. 4(d) and its zoom in 4(g)]. We observe that the oscillations of the plateau have a higher frequency than f_{RO}. In this range of feedback, those fast oscillations create a large number of amplitude extrema corresponding to the scattered area of points in the bifurcation diagram. Finally, for $\eta > 0.078$, only SW without oscillations on the plateaus are observed [Fig. 4(d)]. Furthermore, we notice a bifurcation point H_2 at $\eta = 0.078$ that marks the transition between SW with and without fast oscillations on the plateaus. The frequency observed at H_2 is $f_{H2} = 0.0165$, *i.e.* higher than f_{RO}. This particular point is investigated in the paper.

The spectrogram in Fig. 4(h) summarizes the evolution of the RF spectra when varying η. At the first limit-cycle, for low value of η, the frequency of oscillations remains close to f_{RO} and there is no influence of η in this regime. By contrast, in the SW regime with oscillations on the plateaus, as η increases, the frequency of the oscillations on plateaus also increases; this is in agreement with the experimental observation of Fig. 3(a). As the dynamic does not only consist of a pure oscillatory regime but is also composed of a slower SW modulation, the spectrogram shows a dominant peak for the fast oscillations superimposed on a broad comb of frequency components at multiples of $f_{EC}/2 = 7.1 \times 10^{-5}$. Finally, for $\eta > 0.078$, the dynamic consists of pure SW modulation without oscillation. Therefore, the spectrogram does not show any relevant frequency signature in the high frequency range considered here.

As shown in Fig. 4(a), the fast oscillations on the plateaus have a modulation amplitude that greatly varies as one approaches the bifurcation point H_2. At $\eta = 0.04$, the modulation amplitude of the field intensity $|E_2|^2$ reaches a maximum of 95% of the background SW modulation. In addition, the observed bifurcation scenario is very robust when varying the parameters within the realistic intervals $k = 0.6 - 1$, $T = 150 - 1000$, $P = 0.4 - 2.5$ and $\alpha = 2 - 5$. β is a crucial parameter to observe oscillations on plateaus : increasing its value shrinks the feedback range where those oscillations are observable. Nevertheless, similar dynamics are observable for higher values of both β and pump parameter P. When varying the time delay from 10^3 to 10^4, we do not observe any qualitative change in the sequence of bifurcation leading to the oscillations on plateaus : both the value of the oscillation frequency and its dependency when varying η remain very similar. This is again in agreement with the experiment where the delay had no influence on the frequency of the fast oscillations on plateaus.
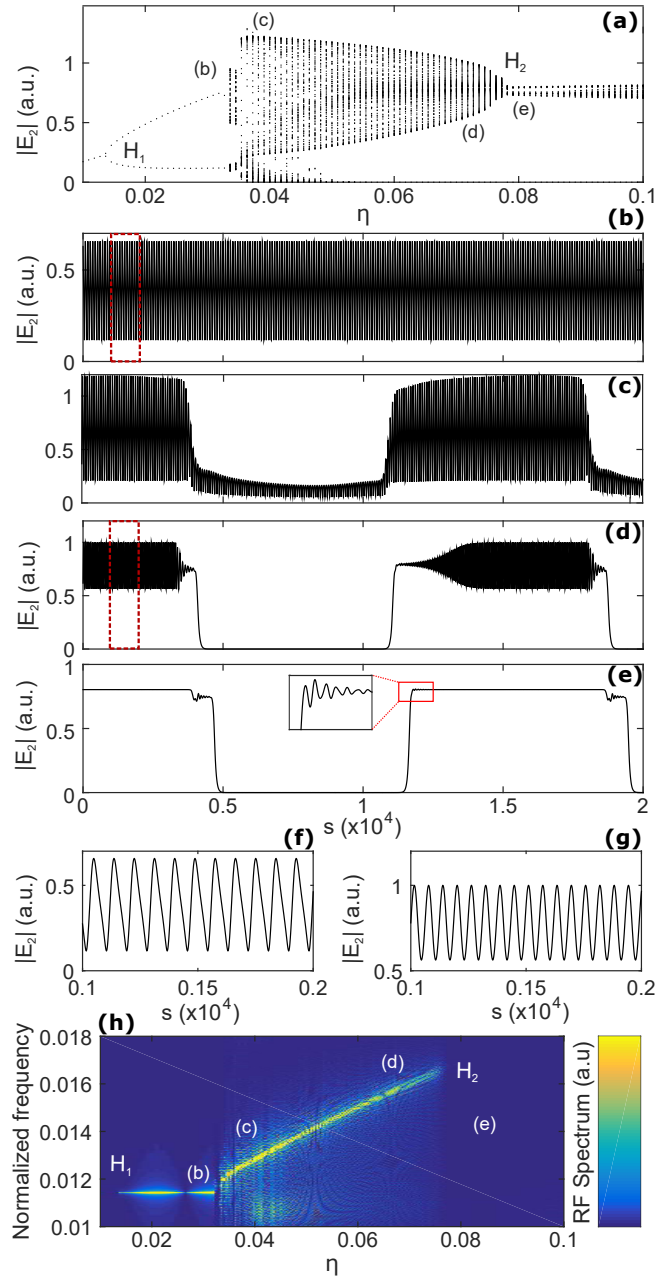
Fig. 4. (a) Numerical bifurcation diagram as function of η. Time traces of $|E_2|$ at (b) $\eta = 0.03$, (c) $\eta = 0.0355$, (d) $\eta = 0.072$, (e) $\eta = 0.08$. (f) and (g) are respectively zooms of (b) and (d) in the dashed box. (h) is the RF spectrogram corresponding to (a).
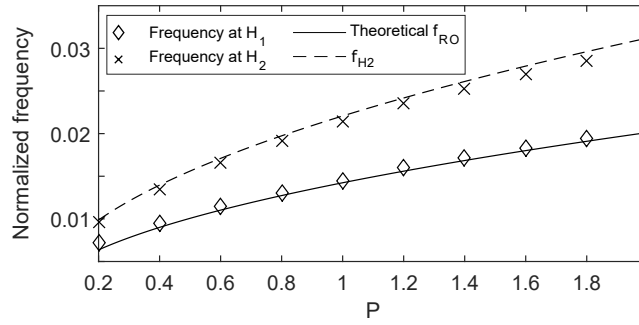
Fig. 5. Numerical and analytical frequency observed at the bifurcation points H_1 and H_2 as function on P using the same parameters as in Fig. 4.

4. Analytical results

To unveil the key parameters driving the evolution of these fast oscillations, we study the stability of the different plateaus of the SW solutions. Because only high-intensity plateau of E_2 destabilizes from Fig. 4(e) to Fig. 4(d), we can restrict the study to these plateaus. Mathematically, this corresponds to the time intervals when $|E_1| = 0$, $N(t - \theta) = 0$, and $|E_1(t - \theta)| = \sqrt{P}$. Substituting these values into Eqs. (1)-(3) leads to the following ODEs

$$\dot{A}_2 = k(N - \beta)A_2 + \eta\sqrt{k}\sqrt{P}\cos(\Phi),$$

$$\dot{\Phi} = -\alpha k(N - \beta) - \eta\sqrt{k}\frac{\sqrt{P}}{A_2}\sin(\Phi),$$

$$T\dot{N} = P - N - (1 + 2N)A_2^2,$$

with $E_j = A_i\exp(j\phi_j)$ $(j = 1, 2)$ and $\Phi = \phi_1(s - \theta) - \phi_2$.

The steady-states of these equations correspond to the values for the variables A_2, Φ and N in the aforementioned time intervals. Next, we look at the Hopf bifurcation responsible for the intability of the plateaus. To simplify, we consider that T is large and, from our simulations, we assume the scalings $N = O\left(T^{-1/2}\right)$; $P = O(1)$; $\beta = O\left(T^{-1}\right)$; $k = O(1)$. The leading order of the Hopf bifurcation conditions gives a simple expressions for the Hopf bifurcation frequency f_{H2}, which reads as

$$f_{H2} = \frac{1}{2\pi}\sqrt{\frac{P}{T}k\left(1 + \alpha^2\right)} = f_{RO}\sqrt{\frac{k}{2}\left(1 + \alpha^2\right)} \tag{4}$$

This expression includes the relaxation oscillation frequency f_{RO} and also a dependency on the linewidth enhancement factor α and the gain ratio k.

In Fig. 5, we represent in dashed line the Hopf bifurcation frequencies f_{H2} obtained from Eq. (4) when varying the pumping current P. We observe a good agreement with the numerical observations of Eqs. (1)-(3) represented by crosses. Even if we considered that β is $O(1/T)$, we note that this assumption gives us a good approximation for the frequency f_{H2}. For comparison purpose, we also show the theoretical value of f_{RO}, the frequency at the Hopf bifurcation H_1 at low feedback rate [$\eta = 0.013$ of Fig. 4(a)]. When increasing P, the frequency at H_1 remains very close to the theoretical value of f_{RO} while the frequency observed at H_2 follows the trend of f_{RO} but remains at a higher value. This is again in agreement with the experimental observation of Fig. 3(b).

Finally, in Fig. 6(a), we show an additional bifurcation scenario for $\alpha = 5$, $\beta = 0.01$ and $k = 0.98$. In Fig. 6(b), the reported H_1 and H_2 bifurcations remain with respectively a frequency
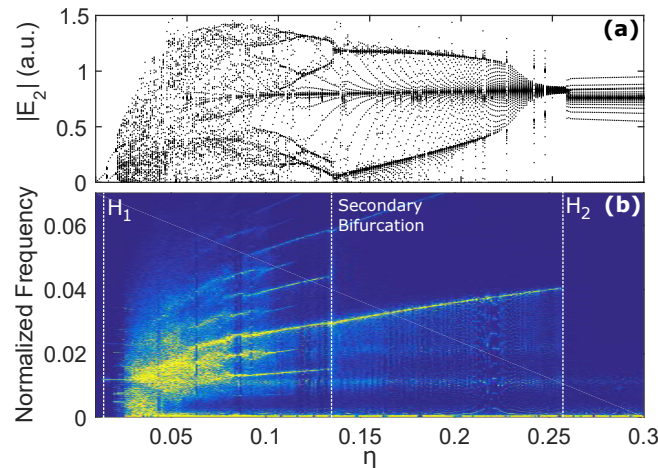
Fig. 6. (a) Bifurcation diagram of $|E_2|$ versus η and (b) the corresponding spectrogram. $\beta = 0.01$, $k = 0.98$ and $\alpha = 5$. The other parameters are identical to those of Fig. 4.

of $f_{H1} = f_{RO} = 0.011$ and $f_{H_2} = f_{RO}\sqrt{\frac{k}{2}\left(1 + \alpha^2\right)} = 0.04$ (3.6 times f_{RO}). However, we observe also a secondary bifurcation at $\eta = 0.13$ arising from the fast oscillations on plateau branch. This bifurcation scenario leads to frequency components in the RF spectrum [Fig. 6(b)] that go well beyond the frequency signatures of f_{RO}, f_{EC} and even higher frequencies than those corresponding to f_{H_2}. For $\tau_p = 1.14$ ps, the situation of Fig. 6(a) leads to oscillations at frequencies above $f_{H_2} = 35$ GHz while $f_{RO} = 9.64$ GHz.

5. Conclusion

In conclusion, we have demonstrated a bifurcation scenario that induces sustained oscillations over a slow polarization switching at a frequency different from the relaxation frequency and from the external-cavity frequency in a laser diode. A polarization-rotated optical feedback induces a slow SW modulation of the laser polarizations and fast oscillations with possibly high modulation amplitude are observed on the upper state of the SW. Interestingly, although the polarization switching dynamics is induced by delayed optical feedback, that self-pulsation frequency does not scale with the time-delay. One could consider long delay i.e. quasi-continuous linear polarization emission and still observe sustained oscillations in the output power. Equation (4) shows that the resulting high-frequency of the fast oscillations has an interesting dependency on both f_{RO} and the linewidth enhancement factor hence suggesting experimentation on different laser devices. A secondary bifurcation on the self-pulsing dynamics may even show frequency components much higher than that given by Eq.(4). More generally, our system shows a dynamics that is made of transition between quiescent and non-stationary states. Such a dynamic in optics has been lately of interest for random number generation [10] and for all-optical flip-flop system [26].

Fundings